Modeling magnetic nanoparticle dipole-dipole interactions inside living cells

Michael Lévy, Florence Gazeau, Jean-Claude Bacri, Claire Wilhelm, and Martin Devaud*

Laboratoire Matière et Systèmes Complexes (MSC), UMR CNRS 7057, Université Paris-Diderot, Bâtiment Condorcet-Case 7056, F-75205 Paris Cedex 13, France

(Received 8 February 2011; revised manuscript received 27 May 2011; published 16 August 2011)

Biomedical applications based on superparamagnetic nanoparticles injected *in vivo* may be affected by the cellular uptake of these nanoparticles. Living cells indeed capture and internalize nanoparticles, concentrating them into intracellular vesicles called lysosomes. As a consequence, nanoparticles interact magnetically with each other, modifying their magnetic properties. The effects of cellular uptake can be observed on the temperature dependence of zero-field cooled (ZFC) magnetization, which is known to be sensitive to magnetic interactions. In this paper, a theoretical model is proposed to account for weak magnetic interactions between nanoparticles aggregated into spherical compartments. This model suggests a new interpretation of the maximum of the ZFC curve, uncorrelated with the nanoparticle relaxation time but with the extent of interaction effects. It focuses on the local field felt by each nanoparticle, which is the sum of the applied magnetic field and the field created by all the other nanoparticles. For the considered organization of nanoparticles, only the field created by touching neighbors has to be taken into account, setting up the local nanoparticle volume fraction as the unique parameter of the model. This parameter relates the global magnetization measurements to the local distribution of nanoparticles in cells and tissues or in other complex media with aggregated organization.

DOI: 10.1103/PhysRevB.84.075480 PACS number(s): 75.75.Jn, 87.85.Tu, 87.55.de

I. INTRODUCTION

Biomedical science develops an increasing number of applications based on the magnetic properties of superparamagnetic nanoparticles (NPs). These applications, such as using superparamagnetic NPs as MRI contrast agents[1,2] or as nanoheaters in magnetic hyperthermia,[3–5] involve injecting NPs into the body. Yet, it has been shown that for a majority of cases, NPs do not stay free in the body. They are captured and internalized by living cells, especially macrophages, sequestering them in intracellular compartments called lysosomes,[6] which are specialized organelles in charge of digesting nonusable substances. Remarkably, in the course of cell internalization, the nanoparticles change their local distribution from dilute NPs in the blood flow to highly concentrated organization inside lysosomes with typical size of 0.2–2 μm. The same intracellular confinement occurs for cells cultured *in vitro* and exposed to magnetic NPs diluted in their extracellular medium. Such a local sequestration of NPs is revealed by transmission electron microscopy (TEM) observations at the nanoscale. While the distribution of NPs is biologically orchestrated at the subcellular level, it may have fundamental consequences on their magnetic behavior. A precise knowledge of NP organization in cells is thus mandatory to optimize their magnetic properties with respect to the considered medical application. Recently we raised the issue that dipolar interparticle interactions may affect the magnetic behavior of NPs sequestered in a lysosome.[7] We indeed observed that the temperature-dependent magnetization was modified by cell internalization of NPs, revealing collective magnetic effects. The maximum of zero-field cooled (ZFC) magnetization was shifted toward higher temperature and its amplitude was decreased for cell-internalized NPs as compared to isolated NPs in colloidal suspension. Interestingly similar phenomena were observed in other complex systems with a mesoscopic organization of NPs.[8–10]

The general approach of this paper is to provide a theoretical framework to describe the magnetic behavior of NPs confined in spherical compartments. A first objective is to link up the magnetic properties of NPs to their local distribution. If the local organization of NPs can be deduced from global magnetization measurements, it could be of primary interest to assess the mesoscopic distribution of NPs in biological samples. Secondly, our approach is the first attempt to delineate the modification of magnetic properties due to cell internalization process. For this purpose and for the sake of simplicity, our analysis is restricted to the interpretation of the ZFC magnetization behavior (at low field), which is sensitive to the whole distribution of relaxation times in the NP assembly with a well-known sensitivity to interparticle magnetic interactions.

Previous experimental and theoretical studies investigated the role of dipole-dipole magnetic interactions on the dynamical behavior of NPs.[8–20] Concerning weak interactions, conflicting models have been proposed. In the Dormann-Bessais-Fiorani (DBF) approach,[11,13] interactions result in an increase of the energy barrier of individual NPs which, as a consequence, increases their magnetic relaxation time. However, the Mørup-Tronc model (MT) using a mean-field approximation, predicts the opposite trend[12,13] with a decrease of relaxation times. Let us notice that these two models analyze the magnetization relaxation time but do not consider the evolution of the magnetization value itself. On the other hand, a third model, known as the interacting superparamagnetic model (ISP), describes the effects of interaction on the magnetization value by adding a phenomenological temperature T^* to the real one.[10,14] This temperature T^* is supposed to mimic the disorder of the NP magnetic moments caused by the random dipolar magnetic field they experiment. It must be noted that these models and the majority of experimental and numerical studies consider concentrated ferrofluids or powders. By contrast, in the present paper, we propose a model to interpret ZFC experiments on compartmentalized NPs which can be regarded as finite aggregates at a submicron scale.

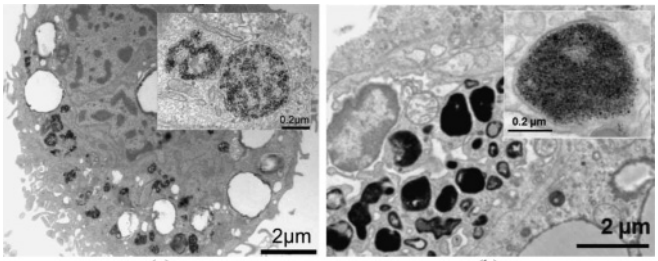

FIG. 1. TEM experiments on the two biological systems. NPs are in dark. (a) TEM on AMNP internalized in macrophages cultured *in vitro*. Magnetic NPs are localized in intracellular vesicles called lysosomes. The inset shows a zoom on a particular lysosome. (b) TEM on P904 NPs internalized in a mouse liver, 3 days after injection. Magnetic NPs are localized in lysosomes, too, which are bigger and more concentrated than in (a). The inset shows a zoom on a particular lysosome.

We analyze the effects of weak interactions on both the relaxation time *and* the magnetization itself. Similarities and differences with previous models are underlined. In particular, our approach suggests a new interpretation of the maximum of the ZFC curve, which is not directly correlated with the NP relaxation time. In addition, we show that this simple experiment, when analyzed within the framework of the present model, can give an assessment of the local distribution of NPs in cells and organs or in other complex systems with aggregated organization.

The present paper is organized as follows. After presenting the experimental results on biological samples (II), we remind the standard theory of ZFC magnetization for noninteracting NPs and apply it to NPs in diluted colloidal suspensions (III). Then we propose an expression for the distribution of local fields experienced by NPs aggregated in a spherical compartment. The consequence of these local fields on the temperature dependence of ZFC magnetization is finally derived (IV) and discussed with respect to other models and experimental results (V).

II. EXPERIMENTS

ZFC magnetization measurements were made on two biological systems representative of most *in vitro* and *in vivo* localizations of iron oxide NPs. On the one hand, the *in vitro* model system consisted of macrophages derived from the activation of human monocytes. These cells were incubated with different concentrations of anionic citrate-coated maghemite NPs (referred to as AMNP) in order to tune the amount of cell-internalized NPs.[21] The internalization pathway of these NPs has been described earlier and their cellular uptake has been quantified by single-cell magnetophoresis.[6,22] TEM pictures of macrophages reveal the intracellular localization of NPs and their confinement into submicron lysosomes[23] [Fig. 1]. On the other hand, similar magnetic NPs (used as MRI contrast agents and referred to as P904) were administrated to mice by intravenous injection. As liver and spleen concentrate large populations of resident macrophages,[24] NPs mainly accumulate in these organs.[25] They are specifically uptaken by macrophages and sequestered within their intracellular lysosomes at remarkably high density as exemplified in Fig. 1(b).

Magnetization measurements were performed on cell suspension or dried organ using a SQUID magnetometer (MPMS XL Quantum Design). The global NP volume fraction ϕ in biological samples was small enough ($\phi \sim 10^{-4} - 10^{-5}$) to neglect any demagnetizing effect linked to their global magnetization. As a comparison, the same measurements were done on the corresponding noninteracting NPs diluted in glycerol ($\phi \sim 10^{-3} - 10^{-4}$). Samples were cooled down to 5 K without any applied field (ZFC), next applying a magnetic field of 50 Gauss and heating slowly up to room temperature, while measuring the magnetization of the sample as a function of temperature. The experimental magnetization M_{exp} was normalized by the maximum magnetization for each sample $M_{\text{max}} = \phi M_s$ which represents the magnetization when all NPs in a unit volume have their magnetic moments aligned in the field direction. Here, M_s is the saturation magnetization of the bulk material at 300 K (we ignore the slight temperature dependence of M_s).

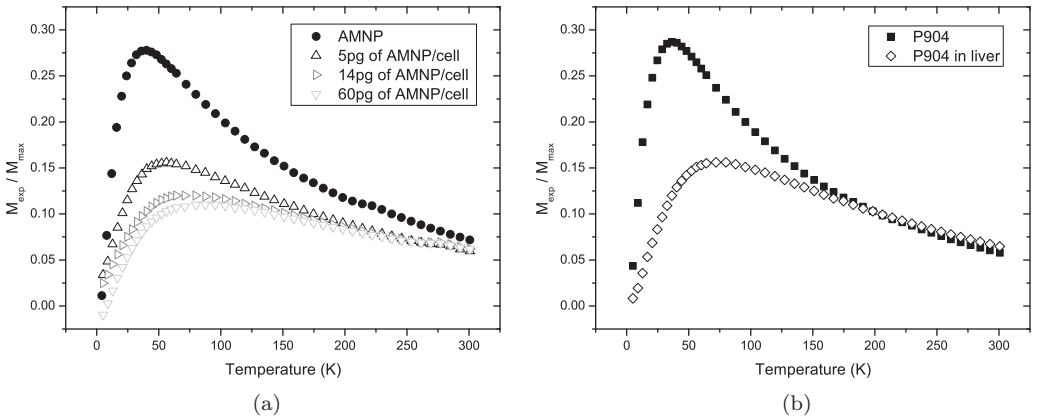

FIG. 2. Reduced magnetization $M_{\text{exp}}/M_{\text{max}}$ in ZFC experiments on (a) AMNP in dilute ferrofluid and internalized in macrophages (the content in AMNP increases from 5 to 60 pg of AMNP per cell); (b) P904 in dilute ferrofluid and internalized in a mouse liver, 3 days after injection.

ZFC magnetization observed in biological systems show clear differences with the corresponding dilute ferrofluid consisting of noninteracting NPs [Figs. 2(a) and 2(b)]:

(1) The magnetization measured in the ZFC experiment is lower for NPs in biological systems than for free NPs and this difference decreases with temperature.

(2) The temperature corresponding to the maximum of the ZFC curve, referred to as the blocking temperature T_B, is higher for NPs in biological systems than in dilute ferrofluids,

(3) More precisely [see Fig. 2(a)], the higher the concentration of internalized nanoparticles, the lower the magnetization and the higher T_B.

It is important to note that NPs are not significantly degraded or transformed by the cells at the time of the experiments (maximum of 3 days postinjection). It has been shown that the metabolization process actually takes a longer time.[25,26] We also verified that the NP size distribution is identical in the dilute suspension and inside the cells. Therefore the modifications of ZFC magnetization compared to noninteracting NPs appear directly linked up to the degree of intracellular confinement of NPs. Consistently with TEM observations, the effects are accentuated in *ex vivo* liver compared to *in vitro* macrophages. The larger the intracellular clustering (which also increased with the cell NP load), the higher the effects on ZFC magnetization. More extensive experiments reported elsewhere[7] show similar modifications depending on cellular sequestration of NPs in different organs. We also verified that NPs enclosed in submicron polymer beads display the same behavior. Similar effects were reported before in other systems with interacting NPs.[8–10] The theory we propose in this paper aims at accounting for these observations. Before presenting it, we first recall in the next section the standard ZFC theory for noninteracting NPs.[27,28]

III. THE STANDARD ZFC THEORY

Let us consider a sample of polydisperse dilute superparamagnetic NPs: Due to the dilution, magnetic interactions between them can be neglected. These NPs are fixed in a solid solvent so that they cannot rotate. The distribution $P(d_m)$ of the particle *magnetic* diameters d_m is described by the log-normal function:

$$P(d_m) = \frac{1}{\sqrt{2\pi}\sigma_m d_m} e^{\left[-\frac{\ln^2(d_m/d_0)}{2\sigma_m^2}\right]}, \tag{1}$$

with d_0 the characteristic *magnetic* diameter and σ_m the polydispersity index (a log-normal function is commonly used to describe the size distribution of NPs synthesized by coprecipitation). Note that the *real* diameter d_r of an NP is considered slightly larger than the magnetic one to take the "nonmagnetic layer" at the surface of the NP and its potential coating into account: $d_r = d_m + 2\delta$, with δ the thickness of the "nonmagnetic layer" plus the coating (δ is typically 1 nm; we suppose it independent of d_m). It will be useful thereafter to define d_{mean} as the mean *real* diameter and μ_{mean} as the magnetic moment of an NP with real diameter d_{mean}:

$$d_{\text{mean}} = \langle d_m + 2\delta \rangle = d_0 e^{2\sigma_m^2} + 2\delta. \tag{2}$$

The particles are supposed to have an uniaxial anisotropy. Let us consider a particular NP with magnetic volume V_m, magnetic moment $\vec{\mu} = M_s V_m \vec{e}$, anisotropy constant K, and easy axis along $\vec{n}$, where $\vec{e}$ and $\vec{n}$ are both unit vectors. In an external magnetic field $\overrightarrow{B_0} = B_0 \vec{u}_z$, the energy U of this NP is given by[29,30]

$$U = -\mu B_0 \vec{e}.\vec{u}_z - K V_m (\vec{e}.\vec{n})^2. \tag{3}$$

In a real sample, the easy-axis $\vec{n}$ is distributed isotropically. Nevertheless, let us momentarily take it along the field direction: $\vec{n} = \vec{u}_z$. The consequence of this approximation is evocated below. Denoting θ the angle between $\vec{e}$ and $\vec{n} = \vec{u}_z$ (see Fig. 3), energy U becomes

$$U = -\mu B_0 \cos\theta - K V_m \cos^2\theta. \tag{4}$$

Then, if B_0 is smaller than $2K/M_s$, that is, if the energy U as a function of θ still has two local minima, and if $k_B T \ll K V_m$, it is possible to use Brown's calculation for the Néel time $\tau_N(d_m, T, B_0)$. The latter represents the relaxation time of the thermally induced transition between the two minima of U, and is given by[31]

$$\frac{1}{\tau_N} = \frac{\gamma^2 \eta 2K}{1 + (\gamma \eta M_s)^2} \sqrt{\frac{\alpha}{\pi}} (1 - \epsilon^2) 2 e^{-\alpha(1+\epsilon^2)} \times \left[\cosh(2\alpha\epsilon) - \epsilon \sinh(2\alpha\epsilon)\right], \tag{5}$$

with $\epsilon = \mu B_0 / 2K V_m$, $\alpha = K V_m / k_B T$, k_B the Boltzmann constant, T the temperature, γ the electron gyromagnetic ratio, and η defined by Brown as a dissipative constant. According to Dormann,[29] the latter can be approximated by $\eta \approx 1/(\gamma M_s)$.

The standard theory for ZFC experiments considers that an NP can be in two different states. If τ_N is larger than the duration τ_{exp} of an experimental measurement, then the magnetic moment is considered blocked (B) in the NP, because the probability for it to fluctuate from one equilibrium position to the other one during time τ_{exp} is very small. On the other hand, if τ_N is smaller than τ_{exp}, the NP is considered superparamagnetic (SP) and its static magnetic behavior is approximated by a Langevin function $\mathcal{L}$. The mean value of the z component of $\vec{\mu}$, that is, what is measured during a ZFC experiment, is then given by

$$\langle \mu_z \rangle (d_m, T, B_0) = \mu \mathcal{L}(\xi_0) = \mu(\coth \xi_0 - 1/\xi_0), \tag{6}$$

with $\xi_0(d_m, T, B_0) = \mu(d_m) B_0 / k_B T$.

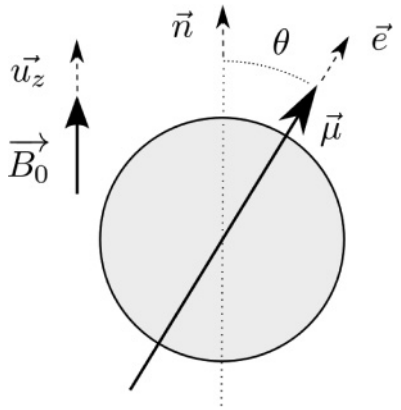

FIG. 3. Magnetic NP with a magnetic moment $\vec{\mu}$ and an easy-axis $\vec{n}$ along the field direction $\vec{u}_z$.

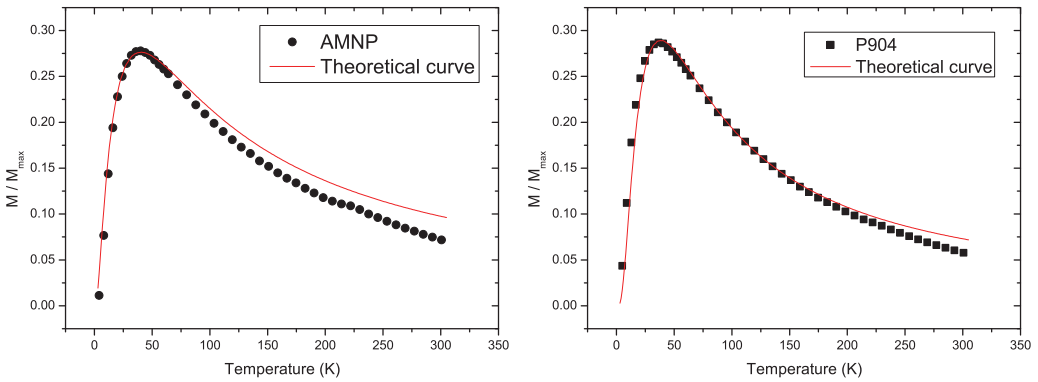

FIG. 4. (Color online) Comparison between the ZFC standard theory and the experiments on dilute ferrofluids. (a) ZFC experiment on AMNP in dilute ferrofluid and corresponding theoretical curve; (b) ZFC experiment on P904 in dilute ferrofluid and corresponding theoretical curve.

In a ZFC experiment, one actually measures $M_z(T)$, the total magnetization of a sample along the applied field direction $\vec{u}_z$: the z components of all magnetic moments should be added and renormalized by the sample volume. The sample was frozen in absence of any field. Then, the magnetic moments of the NPs in the (B) state are isotropically distributed. As a consequence, the latter do not contribute to M_z. Only the magnetic moments of the NPs in the (SP) state at the considered temperature contribute to M_z, adding $\langle\mu_z\rangle(d_m,T,B_0)$ for each of them:

$$M_z(T,B_0) = N\int_{sp(T,B_0)} dd_m\, P(d_m)\langle\mu_z\rangle(d_m,T,B_0), \qquad (7)$$

with N the mean number of NPs per unit volume. As explained above, the integration is made only over the NPs in the (SP) state at the considered temperature T and field B_0, that is, over d_m values smaller than a critical diameter depending on T and B_0. Since the number of these NPs in the (SP) state increases with temperature, M_z starts to increase accordingly. But the contribution to M_z of a given NP in the (SP) state, $\langle\mu_z\rangle(d_m,T,B_0)$, decreases with temperature according to the Langevin function (6). So, when most of the NPs have transited to the (SP) state, $M_z(T)$ starts to decrease. Note that the temperature corresponding to the maximum of $M_z(T)$ (already referred to as the blocking temperature T_B) depends on B_0.

In Figs. 4(a) and 4(b), theoretical as well as experimental curves are plotted for the two dilute ferrofluids. No fitting parameters are used. M_s is taken as the saturation magnetization ($M_s = 412$ kA.m^{-1}) of bulk maghemite, K values are experimentally determined from hysteresis loops at low temperature (5 K) using the Stoner-Wohlfarth model[32] (data not shown), and d_0 and σ_m are deduced from the polydisperse Langevin fits of magnetization curves at room temperature (data not shown). The parameters values are summarized in Table I.

Two comments may be made about the approximations used:

(1) The two dynamical behaviors, blocked (B) or superparamagnetic (SP), respectively, correspond to the two limit cases $\tau_N \gg \tau_{\rm exp}$ and $\tau_N \ll \tau_{\rm exp}$. The approximation that the NPs are either in the (B) state or in the (SP) state (and never in an intermediate one) is justified by the fact that τ_N varies abruptly with the size of the NP (as the exponential of the volume), so that there are very few NPs in an intermediate state. We can therefore introduce the proportions P_{sp} and P_b of NPs in the (SP) and (B) state, respectively:

$$P_{sp}(T,B_0) = \int_{sp(T,B_0)} dd_m\, P(d_m),$$
$$P_b(T,B_0) = 1 - P_{sp}(T,B_0). \qquad (8)$$

(2) As indicated above, the assumption that the easy-axis $\vec{n}$ is in the direction of the field allows us to use the Brown expression (5) for τ_N. For those NPs with an easy axis in another direction, it can be argued that τ_N is shorter. This suggests that the standard theory underestimates the (SP) population. Note that it would be possible to take into account the isotropic easy-axis distribution in the τ_N expression as presented in Refs. 12, 13, 33 and 34. here. Nevertheless, it would complicate the model without modifying the physics. Actually, the standard ZFC theory is often presented using an approximation rougher than (5) for the τ_N expression: $\tau_N \approx \tau_0 e^{\alpha}$, with τ_0 a constant parameter of the order of 10^{-9}. We have preferred expression (5) to keep the field dependence of τ_N.

Despite the approximations made, the standard theory for ZFC experiments on superparamagnetic NPs satisfactorily describe the experimental results for the two dilute ferrofluids. However, this theory evidently fails for the two biological systems as shown by Figs. 2(a) and 2(b). In the present paper, we make and discuss the assumption that this failure is due to the *magnetic interactions* that prevail between the NPs as soon as the latter are internalized in lysosomes.

TABLE I. Sample parameters used for the theoretical calculation.

Sample	d_0(nm)	σ_m	K(J m^{-3})	M_s(kA m^{-1})	δ(nm)
AMNP	6.5	0.33	2.06×10^4	412	1
P904	7.2	0.24	2.47×10^4	412	1

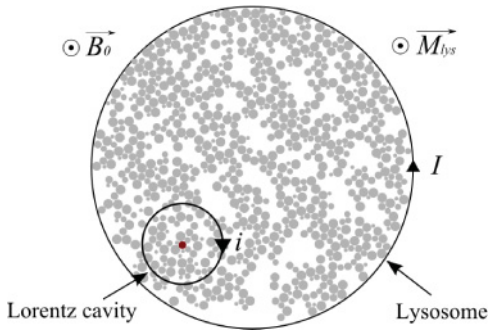

FIG. 5. (Color online) Model of spherical lysosome with a magnetization $M_{\rm lys}$ under an applied magnetic field B_0. The Lorentz cavity around a particular (SP) NP (in dark) is displayed and the surface currents I and i on the surface of the lysosome and of the cavity, respectively, are also represented.

IV. AN ALTERNATIVE THEORY DESIGNED FOR NPS AGGREGATED IN A SPHERICAL COMPARTMENT

A. Modeling of the lysosome

We model the considered lysosomes as spherical compartments nonhomogeneously filled with aggregated NPs (Fig. 5). Let notice that most NPs are touching some neighbors, contrary to an homogeneous concentrated ferrofluid where each NP is separated from its neighbors by some nonzero mean distance. Magnetic interactions between lysosomes are neglected (we consider that the majority of them are separated from each other by more than a mean lysosome diameter).

B. Local magnetic field

As in the standard theory, NPs are considered to be either in the (B) or in the (SP) state, depending on their Néel time τ_N. The latter time τ_N still depends not only on the temperature T, but also on the intensity of the local magnetic field $\overrightarrow{B_{\rm loc}} = B_{\rm loc}\overrightarrow{u_{\rm loc}}$ ($\overrightarrow{u_{\rm loc}}$ unit vector) felt by each given NP. Note that the expression (5) of τ_N we are using still has a meaning as long as the energy U conserves two local minima (i.e., as long as $B_{\rm loc}$ is not too high). That is the reason why the model is limited to *weak interactions*. The restriction induced by this condition will be discussed in Sec. V.

The magnetic moments of the NPs in the (B) state, exactly as in the standard theory, do not contribute to M_z (the number of such NPs in the lysosomes being large enough to average their collective contribution to zero). At the mean-field approximation, NPs in the (SP) state behave according to the Langevin function, but now in the local magnetic field $\overrightarrow{B_{\rm loc}}$ they undergo, and no longer in the mere applied magnetic field $\overrightarrow{B_0}$, which can be written [compare with (6)] as

$$\langle\mu_z\rangle(d_m,T,\overrightarrow{B_{\rm loc}}) = \mu\mathcal{L}(\xi_{\rm loc})\overrightarrow{u_{\rm loc}}.\vec{u_z}, \tag{9}$$

with $\xi_{\rm loc}(d_m,T,B_{\rm loc}) = \mu(d_m)B_{\rm loc}/k_BT$. Observe that $\overrightarrow{B_{\rm loc}}$, contrary to $\overrightarrow{B_0}$, depends on the particular (SP) NP under consideration.

In order to determine $\overrightarrow{B_{\rm loc}}$, the Lorentz method is available. It leads one to introduce a local spherical Lorentz cavity, with center at the considered (SP) NP. The local field $\overrightarrow{B_{\rm loc}}$ is then defined as the field created at the center of the Lorentz cavity by all magnetic field sources *except* this considered (SP) NP. Field $\overrightarrow{B_{\rm loc}}$ can be expressed as a sum of four terms:

(1) $\overrightarrow{B_0}$ the applied magnetic field,

(2) $\overrightarrow{B_I}$ the field created by the surface current I (see Fig. 5) of the lysosome: $\overrightarrow{B_I} = \mu_0\frac{2}{3}\overrightarrow{M_{\rm lys}}$,

(3) $\overrightarrow{B_i}$ the field created by the surface current i (see Fig. 5) of the Lorentz cavity: $\overrightarrow{B_i} = -\mu_0\frac{2}{3}\overrightarrow{M_{\rm lys}}$,

(4) $\overrightarrow{B_n}$ the field created at the center of the Lorentz cavity by the neighbors (n) located inside this Lorentz cavity, when $\overrightarrow{B_0}$ is applied. $\overrightarrow{B_n}$ is itself the sum of two contributions: one ($\overrightarrow{B_b}$) from the neighbors being in the (B) state and one ($\overrightarrow{B_{sp}}$) from the neighbors being in the (SP) state: $\overrightarrow{B_n} = \overrightarrow{B_b} + \overrightarrow{B_{sp}}$. Note that, contrary to what turns out when the contributions of *all* the NPs of the *whole* lysosome in the (B) state are summed up (as explained above), $\overrightarrow{B_b}$ is now *nonzero*: There are *too few* neighbors in the (B) state to average $\overrightarrow{B_b}$ to zero.

Because of the spherical symmetry of the lysosome, $\overrightarrow{B_I} = -\overrightarrow{B_i}$ (i.e., the resulting effect of magnetic interactions in the lysosome is consequently only due to the neighbors *inside* the Lorentz cavity): $\overrightarrow{B_{\rm loc}} = \overrightarrow{B_0} + \overrightarrow{B_n}$.

When $\overrightarrow{B_0}$ is not applied, the neighbors inside the Lorentz cavity create a field $\overrightarrow{B_n^0}$ which is still the sum of two contributions $\overrightarrow{B_b^0}$ and $\overrightarrow{B_{sp}^0}$ from the neighbors in the (B) and the (SP) state, respectively. Let $\overrightarrow{B_{\rm loc}^0} = \overrightarrow{B_0} + \overrightarrow{B_n^0} = B_{\rm loc}^0\,\overrightarrow{u}^0_{\rm loc}$ ($\overrightarrow{u}^0_{\rm loc}$ unit vector) be the local magnetic field felt by the NP at the center of the Lorentz cavity when $\overrightarrow{B_0}$ is not applied.

(1) Since $\mu B_0/KV_m$ is of the order of 10^{-2}, the NPs in the (B) state are not affected by $\overrightarrow{B_0}$. Thus, they create the same field in the presence or absence of $\overrightarrow{B_0}$: $\overrightarrow{B_b} = \overrightarrow{B_b^0}$ ($\neq 0$ as explained above).

(2) However, the NPs in the (SP) state (and therefore the field $\overrightarrow{B_{sp}}$ they create) are affected by $\overrightarrow{B_0}$. Let us consequently set $\overrightarrow{B_{sp}} = \overrightarrow{B_{sp}^0} + \overrightarrow{\delta B}$ with $\overrightarrow{\delta B} = \delta B\overrightarrow{u_{\delta B}}$ ($\overrightarrow{u_{\delta B}}$ unit vector).

Using these definitions and the above remarks (1) and (2), we have

$$\begin{aligned}\overrightarrow{B_{\rm loc}} &= \overrightarrow{B_0} + \overrightarrow{B_b} + \overrightarrow{B_{sp}}\\ &= \overrightarrow{B_0} + \overrightarrow{B_n^0} + \overrightarrow{\delta B}\\ &= \overrightarrow{B_{\rm loc}^0} + \overrightarrow{\delta B}.\end{aligned} \tag{10}$$

Assuming that $\overrightarrow{B_n^0}$ and $\overrightarrow{\delta B}$ are uncorrelated, with probability densities $P(\overrightarrow{B_n^0})$ and $P(\overrightarrow{\delta B})$, respectively, the total magnetization $M_z(T,B_0)$ of the sample can be expressed as [compare with (7)]

$$\begin{aligned}M_z(T,B_0) = N\int d^3B_n^0 P(\overrightarrow{B_n^0})\int d^3\delta B\,P(\overrightarrow{\delta B})\int_{sp(T,B_{\rm loc})}\\ \times\, dd_m P(d_m)\langle\mu_z\rangle(d_m,T,\overrightarrow{B_n^0},\overrightarrow{\delta B}).\end{aligned} \tag{11}$$

Note that $\langle\mu_z\rangle$ depends on $\overrightarrow{B_{\rm loc}}$ [see (9)]; then, it can be expressed either as a function of $\overrightarrow{B_n^0}$ and $\overrightarrow{\delta B}$ [$\langle\mu_z\rangle(d_m,T,\overrightarrow{B_n^0},\overrightarrow{\delta B})$ like in the above Eq. (11)] or as a function of $\overrightarrow{B_{\rm loc}^0}$ and $\overrightarrow{\delta B}$

$[\langle\mu_z\rangle(d_m,T,\overrightarrow{B^0_{\rm loc}},\overrightarrow{\delta B})$ like in Eq. (13) below], for the sake of calculation convenience.

C. Approximations on δB and $P(\delta B)$

The mean-field intensity created around a magnetic moment μ at a distance r is given by

$$B_m(\mu,r)=\frac{\mu_0}{4\pi}\frac{\sqrt{2}\mu}{r^3}. \tag{12}$$

According to (12), the mean-field intensity created at a distance $r=d_{\rm mean}$ around a typical nanoparticle considered in this paper is of the order of 300 Gauss. As a consequence, the applied field $\overrightarrow{B_0}$ (50 Gauss) should have just a small influence on $\overrightarrow{B_{sp}}$. So we can assume that $\delta B \ll B^0_{\rm loc}$.

According to (9), we can expand $\langle\mu_z\rangle(d_m,T,\overrightarrow{B^0_{\rm loc}},\overrightarrow{\delta B})$ at the (included) first order in $\delta B/B^0_{\rm loc}$:

$$\langle\mu_z\rangle\left(d_m,T,\overrightarrow{B^0_{\rm loc}},\overrightarrow{\delta B}\right)\simeq\mu\Bigg[\mathcal{L}\left(\xi^0_{\rm loc}\right)\overrightarrow{u}^0_{\rm loc}.\overrightarrow{u_z}+\overrightarrow{\delta B}.\times\left(\frac{\partial}{\partial\overrightarrow{B_{\rm loc}}}\left(\mathcal{L}(\xi_{\rm loc})\overrightarrow{u}_{\rm loc}.\overrightarrow{u_z}\right)\right)_{\overrightarrow{\delta B}=0}\Bigg], \tag{13}$$

with $\xi^0_{\rm loc}(d_m,T,B^0_{\rm loc})=\mu(d_m)B^0_{\rm loc}/k_BT$.

Because of the random position of the NPs in the (SP) state inside the Lorentz cavity, the probability density $P(\overrightarrow{\delta B})$ of $\overrightarrow{\delta B}$ is assumed isotropic: $P(\overrightarrow{\delta B})=P(\delta B)$. Then, the integration over the angular components of $\overrightarrow{\delta B}$ in (11) cancels the contribution of the first-order term in the right-hand side of (13). The only term that contributes to M_z is therefore the zero-order term.

On the other hand, because $\overrightarrow{B^0_n}$ is the field created by the neighbors when $\overrightarrow{B_0}$ is not applied, there is no privileged direction and the probability density $P(\overrightarrow{B^0_n})$ is isotropic too (as assumed in the MT model[12,13]). Then Eq. (11) becomes (B^0_n,θ_0,ϕ_0) standing for the spherical coordinates of $\overrightarrow{B^0_n}$:

$$M_z(T,B_0)=N\int_0^\infty dB^0_n\left(B^0_n\right)^2P\left(\overrightarrow{B^0_n}\right)\int_0^\pi d\theta_0 2\pi\sin\theta_0\int_{sp(T,B^0_n)}\times dd_m\,P(d_m)\mu(d_m)\mathcal{L}\left(\xi^0_{\rm loc}\right)\frac{B^0_n\cos\theta_0+B_0}{B^0_{\rm loc}}, \tag{14}$$

with

$$B^0_{\rm loc}=\left(\left(B^0_n\right)^2+2B^0_nB_0\cos\theta_0+B_0^2\right)^{\frac{1}{2}}. \tag{15}$$

D. Determination of an approximate expression for $P\left(B^0_n\right)$

We should now determine $P(\overrightarrow{B^0_n})$. All neighbors localized in the Lorentz cavity contribute in principle to $\overrightarrow{B^0_n}$. Nevertheless, we can assume that the closer they are to the center of the Lorentz cavity, the more they contribute to $\overrightarrow{B^0_n}$ for the following reason. The field created by an infinity of magnetic (or electric) dipoles uniformly located on the surface of a sphere and having either the same direction or a random one, is equal to zero at the center of the sphere. In our case, if we consider populations of neighbors at a given distance from the center of the Lorentz cavity, the shorter this distance is, the smaller the corresponding population is and the farther we are from this theoretical case where all dipoles cancel each other's contribution to the field. Moreover, the closest neighbors create, at the center of the Lorentz cavity, a field much more inhomogeneous than the other neighbors (because of the r^{-3} dependence of a dipolar field) which has no chance at all to be compensated.

In this study, we will thus take only the "touching" neighbors (in direct contact) into account, considering that they are responsible for the largest part of $\overrightarrow{B^0_n}$. An improvement of our model would be to take more neighbors into account, but we do not think that it would much change the physics of the problem.

At a given temperature T, let $N_b(T)$ and $N_{sp}(T)$ be the mean number of touching neighbors in the (B) and the (SP) state, respectively, $d_b(T)$ and $d_{sp}(T)$ be the mean real (i.e., including the nonmagnetic layer) diameters of these NPs in the (B) and the (SP) states, respectively, and $P_b(T)$ and $P_{sp}(T)$ be the probabilities of being in the (B) and in the (SP) state, respectively, ($P_b(T)$ and $P_{sp}(T)$ as displayed by (16) below represent a simple generalization of (8). Let ρ be the mean neighbor volume fraction (note that ρ is a very local volume fraction concerning only these touching neighbors).

Then, $N_b(T)$ and $N_{sp}(T)$ can easily be calculated as follows.

(1) The volume in which the (B) or (SP) neighbors are included is determined [e.g., the (SP) neighbors are included in a volume equal to $(3d_{sp})^3\pi/6-d^3_{sp}\pi/6=26d^3_{sp}\pi/6$].

(2) Next, the latter volume is multiplied by ρ to get the total volume occupied by the NPs.

(3) We then divide by the mean NP volume $d^3_{\rm mean}\pi/6$ to get the corresponding number of neighbors.

(4) At last, multiplying by the proportion P_{sp} or P_b of NPs in the (SP) or the (B) state, respectively, we obtain $N_{sp}(T)$ and $N_b(T)$.

$$\begin{aligned}N_{sp}(T)&=\frac{26\rho}{d^3_{\rm mean}}d^3_{sp}P_{sp}(T),\\ P_{sp}(T)&=\int d^3B^0_nP\left(\overrightarrow{B^0_n}\right)\int_{sp(T,B^0_n)}P(d_m)dd_m,\\ N_b(T)&=\frac{\rho}{d^3_{\rm mean}}\left((2d_b+d_{sp})^3-d^3_{sp}\right)P_b(T),\\ P_b(T)&=1-P_{sp}(T).\end{aligned} \tag{16}$$

In order to determine an approximate expression for $P(\overrightarrow{B^0_n})$, $\overrightarrow{B^0_n}$ is again considered as the sum of $\overrightarrow{B^0_b}$ and $\overrightarrow{B^0_{sp}}$ where $\overrightarrow{B^0_b}$ and $\overrightarrow{B^0_{sp}}$ are now, according to our assumption, the fields created by the *mere* touching neighbors in the (B) and the (SP) state, respectively. Our calculation of $P(\overrightarrow{B^0_n})$ involves the following three steps (detailed below): First, the probability densities $P(B^0_{bi})$ and $P(B^0_{spi})$ of the i component of $\overrightarrow{B^0_b}$ and $\overrightarrow{B^0_{sp}}$, respectively, are calculated (with i being x, y, or z); then, the probability density $P(B^0_{ni})$ of the i component of $\overrightarrow{B^0_n}$ is deduced; and finally $P(\overrightarrow{B^0_n})$ is evaluated. Let us detail this three-step calculation.

Step 1. We provisionally focus on $P(B_{bi}^0)$ for the sake of simplicity. Let us consider that each neighbor in the (B) state contributes to B_{bi}^0 by simply *adding* or *subtracting* a constant $\mathcal{B}_b = B_m(\mu_b, r_b)/\sqrt{3}$ [see (12)] with r_b the mean center-to-center distance: $r_b = (d_{sp} + d_b)/2$ and μ_b the mean magnetic moment of the NPs in the (B) state:

$$\mu_b = \int d^3 B_n^0 P\left(\overrightarrow{B_n^0}\right) \frac{\int_{b(T,B_n^0)} dd_m P(d_m)\mu(d_m)}{\int_{b(T,B_n^0)} dd_m P(d_m)}. \quad (17)$$

More precisely, let n_+ be the number of (B) neighbors which contribute to B_{bi}^0 by adding $\mathcal{B}_b$, n_- the number of (B) neighbors which contribute to B_{bi}^0 by subtracting $\mathcal{B}_b$, and $m = n_+ - n_-$ the difference between these numbers. Thus, $B_{bi}^0 = m\mathcal{B}_b$. The probability density $P(B_{bi}^0)$ is then equivalent to the probability density of m, $P(m)$.

Another approximation is required to evaluate $P(m)$. As exposed above, if there were enough touching neighbors in the (B) state (they then should have an infinitely small size and constitute a shell), the field created by these (B) touching neighbors at the center of the Lorentz sphere would be exactly zero. In fact, the nonzero field $\overrightarrow{B_b^0}$ results from a "poor" statistics: The number of neighbors in the (B) state is *too small* to average it to zero. Consequently, $\overrightarrow{B_b^0}$ can be treated as a statistical fluctuation which goes to zero when there are enough neighbors in the (B) state. Let $\mathcal{N}$ be the minimum number of (B) neighbors such that the sum of their contributions to $\overrightarrow{B_b^0}$ can reasonably be considered equal to 0. We can now add the following condition: if $N_b = \mathcal{N}$ then $m = 0$.

With this condition, $P(m)$ is given by

$$P(m) = \frac{N_b!}{\left(\frac{N_b-m}{2}\right)!\left(\frac{N_b+m}{2}\right)!} \frac{(\mathcal{N}-N_b)!}{\mathcal{N}!} \frac{\left(\frac{\mathcal{N}}{2}\right)!}{\left(\frac{\mathcal{N}}{2}-\frac{N_b-m}{2}\right)!} \times \frac{\left(\frac{\mathcal{N}}{2}\right)!}{\left(\frac{\mathcal{N}}{2}-\frac{N_b+m}{2}\right)!}. \quad (18)$$

The Stirling formula on the Taylor development of $\ln[P(m)]$ at the second order in m leads to express $P(m)$ as a normal distribution with a standard deviation σ given by $\sigma^2 = N_b(\mathcal{N} - N_b)/\mathcal{N}$. Consequently, an approximate expression of $P(B_{bi}^0)$ is found:

$$P(B_{bi}^0) = \frac{1}{\sqrt{2\pi}\sigma_b} e^{-(B_{bi}^0)^2/2\sigma_b^2} \quad \text{with} \quad \sigma_b^2 = \frac{\mathcal{B}_b N_b(\mathcal{N}-N_b)}{\mathcal{N}}. \quad (19)$$

The first step of the calculation can be carried all the same with the (SP) touching neighbors, in order to determine the probability density $P(B_{spi}^0)$. The arguments are mostly the same. We just have to substitute index "sp" for "b". The only differences concern the mean center-to-center distance $r_{sp} = d_{sp}$ and the mean magnetic moment μ_{sp} of the NPs in the (SP) state which is slightly different from μ_b to take the thermal fluctuations into account:

$$\mu_{sp} = \int d^3 B_n^0 P\left(\overrightarrow{B_n^0}\right) \frac{\int_{sp(T,B)} dd_m P(d_m)\mu(d_m)\mathcal{L}\left(\xi_{\text{loc}}^0\right)}{\int_{sp(T,B)} dd_m P(d_m)}. \quad (20)$$

We then get expressions of $P(B_{spi}^0)$ and σ_{sp}^2 analogous to (19). As a conclusion, $\overrightarrow{B_{sp}^0}$ (just like $\overrightarrow{B_b^0}$) can be regarded as a statistical fluctuation that goes to zero when there are enough neighbors in the (SP) state.

Step 2. Because $B_{ni}^0 = B_{bi}^0 + B_{spi}^0$, the probability density of B_{ni}^0 can be derived from $P(B_{bi}^0)$ and $P(B_{spi}^0)$:

$$P(B_{ni}^0) = \int_{-\infty}^{+\infty} dB_{bi}^0 \int_{-\infty}^{+\infty} dB_{spi}^0 P\left(B_{bi}^0\right) P\left(B_{spi}^0\right) \delta\left(B_{ni}^0 - B_{bi}^0 - B_{spi}^0\right) = \frac{1}{\sqrt{2\pi\left(\sigma_b^2 + \sigma_{sp}^2\right)}} e^{-(B_{ni}^0)^2/2(\sigma_b^2+\sigma_{sp}^2)}, \quad (21)$$

according to (19) and to its equivalent for (SP) neighbors.

Step 3. At last, the probability density $P(\overrightarrow{B_n^0})$ can be calculated.

$$P(\overrightarrow{B_n^0}) = P\left(B_{nx}^0\right) P\left(B_{ny}^0\right) P\left(B_{nz}^0\right) = \frac{1}{\left(2\pi\left(\sigma_b^2 + \sigma_{sp}^2\right)\right)^{\frac{3}{2}}} e^{-(B_n^0)^2/2(\sigma_b^2+\sigma_{sp}^2)}. \quad (22)$$

It is noteworthy that we justify here an approached Gaussian distribution for $\overrightarrow{B_n^0}$ which is *assumed* in the MT model.[12,13] Now, all functions appearing in the expression (14) of $M_z(T)$ are defined. The three integrations on d_m, B_n^0, and θ_0 can be performed numerically. The reader not interested in the way the numerical resolution is carried out can jump to the next section.

E. Numerical resolution

The above theory deserves a further comment. According to (16), (17), and (20), $P(\overrightarrow{B_n^0})$ is needed to calculate $N_b(T)$, $N_{sp}(T)$, $\mu_b(T)$, and $\mu_{sp}(T)$. But according to (19) and (22), $N_b(T)$, $N_{sp}(T)$, $\mu_b(T)$, and $\mu_{sp}(T)$ are also needed to calculate $P(\overrightarrow{B_n^0})$. This entangled problem can be solved perturbatively. For the lowest temperature, $T_0 = 3K$, all neighbors are supposed to be in the (B) state (at the zero order of our perturbative resolution): $N_b(T_0) = 26\rho$, $N_{sp}(T_0) = 0$, $\mu_b(T_0) = \mu_{\text{mean}}$ [as indicated after Eq. (2), μ_{mean} is the magnetic moment of an NP with real diameter d_{mean}) and $\mu_{sp}(T_0) = 0$. Then, $P(\overrightarrow{B_n^0})$ can be calculated. This zero-order $P(\overrightarrow{B_n^0})$ is then used to calculate more accurately $N_b(T_0)$, $N_{sp}(T_0)$, $\mu_b(T_0)$, and $\mu_{sp}(T_0)$ at the first order. These new values give in turn a more accurate $P(\overrightarrow{B_n^0})$ (at the first order) which is used in (14) to evaluate $M_z(T_0)$. Then, for the next temperature, $T_0 + \Delta T$, the same approach is used with $N_b(T_0)$, $N_{sp}(T_0)$, $\mu_b(T_0)$, and $\mu_{sp}(T_0)$ at the first order playing the role of $N_b(T_0 + \Delta T)$, $N_{sp}(T_0 + \Delta T)$, $\mu_b(T_0 + \Delta T)$, and $\mu_{sp}(T_0 + \Delta T)$ at the zero order. This method is iterated for all temperatures T_i. Using the values calculated at T_i at the first order to evaluate them at T_{i+1} at the zero order is justified if $\Delta T = T_{i+1} - T_i$ is small enough toconsider that very few NPs change their state from (B) to (SP) between T_i and T_{i+1}. In the following theoretical results, ΔT is taken equal to 1 K.

V. RESULTS AND DISCUSSION

A. Experimental observations are predicted by the model

Figure 6(a) displays ZFC theoretical curves with ρ increasing from 0 (noninteracting NPs) to 0.2. We observe that

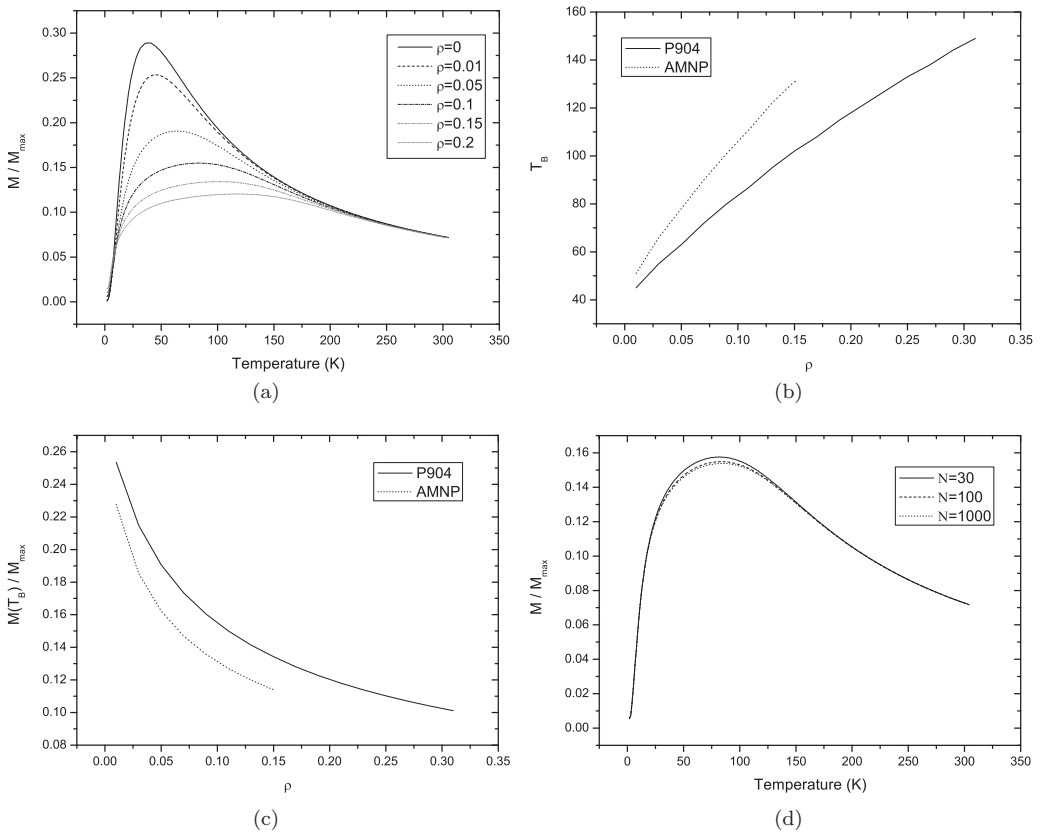

FIG. 6. The model predicts the experimental observations. (a) ZFC theoretical curves for different ρ values using the P904 parameters, (b) theoretical blocking temperature T_B as a function of ρ for AMNP and P904, (c) theoretical normalized magnetization $M(T_B)$ at blocking temperature as a function of ρ for AMNP and P904, (d) ZFC theoretical curves for $\rho = 0.1$ and different $\mathcal{N}$ values; the curves do not depend on $\mathcal{N}$.

the trends found in the *in vitro* and *in vivo* experiments are reproduced by the theoretical model.

First, the larger ρ, the more shifted the blocking temperature T_B. This behavior is represented in Fig. 6(b) where the theoretical T_B is plotted as a function of ρ for the P904 and AMNP samples. The increase of T_B is almost linear with ρ.

Second, the magnetization is found lower for interacting NPs ($\rho \neq 0$) than for noninteracting ones. As in experiments, this effect increases with ρ but decreases at high temperature. Figure 6(c) displays the theoretical magnetization at T_B, $M(T_B)$, renormalized per $M_{\max}$, as a function of ρ for both P904 NPs and AMNP.

In the above-exposed theory, $\mathcal{N}$ and ρ are two unknown parameters. But actually, as long as $\mathcal{N}$ is much larger than the total number of touching neighbors, its value does not really matter. To illustrate this point, ZFC theoretical curves for three $\mathcal{N}$ values ($\mathcal{N} = 30$, $\mathcal{N} = 100$, $\mathcal{N} = 1000$) are displayed in Fig. 6(d) in which we set $\rho = 0.1$ and use the parameters of the P904 sample: The three curves are hardly distinguishable. The local NP volume fraction ρ is thus the unique relevant unknown parameter in this model. We conclude that, according to the model, the ZFC response of our interacting system is only sensitive to the very local NP distribution rather than to the global NP density or to the lysosome size, for instance. Experiments made on samples containing different sizes of spherical submicron polymer assembly of NPs and yet resulting in a very similar effect confirm this independency in the global aggregate size (data not shown). The experimental ρ value can be deduced comparing the experimental results and the model predictions. We can then access to a parameter which characterizes *in situ* the intracellular organization of NPs by means of a simple macroscopic experiment. A study focusing on the biological interest of such information is presented elsewhere.[7]

Let us add that, in the model exposed here, the ρ value and then the total number of touching neighbors is fixed: It is considered the same for all NPs. Yet, in real biological systems, this number is obviously distributed following an unknown probability density. Consequently we only access to an average value.

B. Study of the local magnetic field and its consequences

It is of interest to study the real local field felt by the NPs and its evolution with ρ and with temperature. To do so, let us investigate the behavior of the mean intensity B_{mean} of $\overrightarrow{B_{\text{loc}}^0} = \overrightarrow{B_0} + \overrightarrow{B_n^0}$. Considering $\delta B \ll B_{\text{loc}}^0$, $\overrightarrow{B_{\text{loc}}^0}$ is indeed almost the real field felt by the NPs and B_{mean} gives an idea of its intensity:

$$B_{\text{mean}}(T, B_0) = \int d^3 B_n^0 P\left(\overrightarrow{B_n^0}\right) B_{\text{loc}}^0, \tag{23}$$

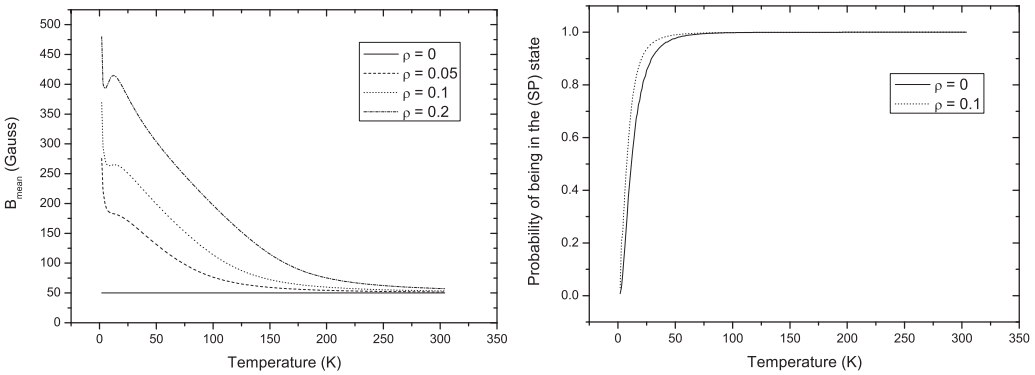

(a) (b)

FIG. 7. Theoretical study of the local magnetic field and its consequences on the (B)-(SP) transition using the P904 parameters. (a) $B_{\text{mean}}(B_0 = 50$ Gauss) as a function of the temperature for different ρ values; (b) probability of being in the (SP) state as a function of temperature.

with B^0_{loc} given by (15). In Fig. 7(a) we have plotted $B_{\text{mean}}(B_0 = 50$ Gauss) as a function of temperature for three values of ρ and with the P904 parameters. It appears that B_{mean} is always larger than B_0 and tends toward B_0 at high temperature. At very low temperatures, all neighbors are in the (B) state, and they contribute to B_{loc} with their total magnetic moment μ [according to (17)]. When the temperature increases, NPs quickly change their state from (B) to (SP). As a consequence, the contribution of the (SP) neighbors arises and increases while the contribution of the (B) neighbors decays. This transition sparks off the little peak that appears at low temperature when ρ increases. Nanoparticles in the (SP) state contribute to B_{loc} not with their total magnetic moment μ but with a magnetic moment $\mu\mathcal{L}(\xi^0_{\text{loc}})$ to take thermal fluctuations into account [according to (20)]. Yet, $\mu\mathcal{L}(\xi^0_{\text{loc}})$ decreases with temperature. The interaction effect is thus weaker at high temperatures and B_{mean} tends toward B_0.

Let us add that, in the theory developed here, B_{loc} has to be always smaller than $2K/M_s$ (around 1100 Gauss) for the τ_N expression (5) to be usable, as specified in the standard theory section. This limitation imposes an upper limit on the local volume fraction ρ (between 0.2 and 0.3 with the parameters used here). For larger ρ values, the theory cannot be applied; we should then consider the "strong interaction" framework.[18,35]

We have remarked that B_{mean} is always larger than B_0 (i.e., the majority of NPs feel a magnetic field $\overrightarrow{B_{\text{loc}}}$ whose intensity is larger than B_0). The Néel time τ_N, which depends on the intensity of the local magnetic field $\overrightarrow{B_{\text{loc}}}$, is then affected. Actually, τ_N decreases as B_{loc} increases according to the MT model.[12,13] Thus, the higher B_{loc}, the lower the temperature transition between the (B) and the (SP) state. In this sense, NPs internalized in lysosomes should transit from (B) to (SP) at a lower temperature than NPs in dilute ferrofluids. This is illustrated in Fig. 7(b) where the probability for an NP to be in the (SP) state is displayed as a function of temperature for $\rho = 0$ and $\rho = 0.1$. Such decrease of the temperature transition should induce a decrease of T_B and, yet, we observe experimentally and theoretically the opposite trend. To understand this effect we separate in the next section the contribution of each size of NP to the total magnetization.

C. Study of different populations of NPs with specific sizes

Let us consider the magnetization of a specific population of NPs with a fixed diameter. They are still considered surrounded by polydisperse nanoparticles interacting with them. Figure 8 displays the magnetization of two of these specific populations (with magnetic diameters $d_m = d_{\text{mean}} =$ 7.5 nm and $d_m = 10$ nm) renormalized per their maximum magnetization.

It can be observed that, for the two considered populations, the magnetization is lower with interaction than without interaction. This effect comes from the fact that $\overrightarrow{B_{\text{loc}}}$ can be oriented in all directions, so it imposes on (SP) NPs to align their magnetic moments in different directions [see (9)] reducing their contribution along the applied field $\overrightarrow{B_0}$. Note that in the ISP model, this phenomenon is taken into account adding a phenomenological temperature T^* to increase the magnetic moment disorder as reminded in Sec. I.

The surprising shift of T_B in the presence of interaction can be explained focusing on the magnetic behavior of the

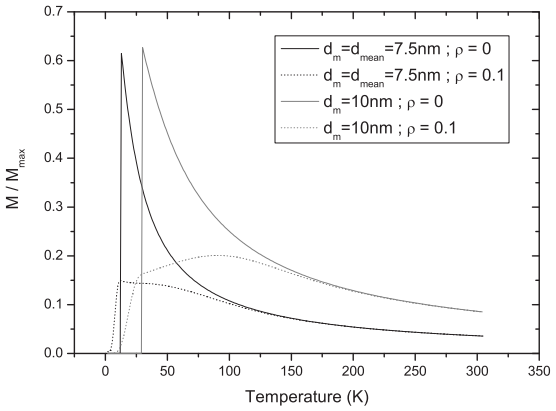

FIG. 8. Theoretical normalized magnetization of two different NP populations ($d_m = d_{\text{mean}} = 7.5$ nm and $d_m = 10$ nm) with fixed magnetic diameter in both cases without ($\rho = 0$) and with ($\rho = 0.1$) interaction. They are considered in a lysosome, surrounded by polydisperse nanoparticles interacting with them but only their contribution to the total magnetization is plotted.

population with $d_m = 10$ nm in Fig. 8. The presence of a maximum for a temperature much higher than the temperature of the (B)-(SP) transition on the curve with interaction is the source of the high T_B value. This maximum can be apprehended in the following way. When the temperature increases, the (SP) contribution to B_{loc} decreases (as underlined above), and consequently the interaction effect decreases [see also the decrease of B_{mean} in Fig. 7(a)]. The magnetization gets closer to its value without interaction, and thus it can increase to reach this value if the difference between the magnetizations with and without interaction is high enough. This increase produces a maximum which has nothing to do with the (B)-(SP) transition: It is only the consequence of the interaction effect decrease with temperature, contrary to the usual interpretation which considers the T_B increase as a signature of a slowing down of the magnetic moment dynamics.[11,17–20] The above analysis represents then a new interpretation of the maximum of the ZFC curve (poorly correlated with the NP relaxation time) which could presumably be generalized to AC measurements, too.

Let us note that there is not a maximum at high temperature for all populations of NPs with interactions. For example, the population with $d_m = d_{\text{mean}} = 7.5$ nm in Fig. 8 does not present such a maximum. The presence of a maximum at high temperature is based indeed on the decrease of the (SP) contribution to B_{loc}. If a population with a too small size is considered, the (B) contribution to B_{loc} dominates the (SP) contribution up to a temperature for which the difference between the magnetization with and without interaction is too small to produce an increase of the magnetization with interaction. In this case, no maximum is likely to be found.

A last observation can be made about Fig. 8. It appears that the increase of magnetization at low temperature is less abrupt with interaction than without interaction. In the latter case (i.e., without interaction), the magnetization of the population is zero until (B) NPs become (SP). Then all NPs contribute the same way according to (6). They all become (SP) at the same temperature because they all have the same Néel time. In the former case (i.e., with interaction), there is a distribution of Néel times for each temperature because of the distribution of $\overrightarrow{B_{\text{loc}}}$. NPs become (SP) at different temperatures, depending on the local field they feel. Moreover, they become (SP) mostly at a lower temperature than in the case without interaction because this local field is generally larger than B_0 as explained above. This is why the increase of the magnetization at low temperature is less abrupt with interaction than without interaction and why it occurs for a lower temperature.

VI. CONCLUSION

The theoretical "weak interaction" model exposed here describes a very specific experimental system and this specificity allows some simplifications. For example, the fact that the total volume fraction ϕ is small and the lysosome is assumed spherical allows us to neglect all interaction sources except neighbors inside the Lorentz cavity. For a larger ϕ value or/and another system geometry, global interaction effects should be taken into account (as the demagnetizing field). Nevertheless, concerning the specific biological case of magnetic NPs internalized in lysosomes, the system described here seems quite general: In different types of cells or in different organs, the same simplifications should be possible.

According to this model the local field felt by intralysosomal NPs is approximately described by a well-characterized isotropic Gaussian distribution. Moreover, the unique relevant parameter influencing the magnetic response of our interacting systems is the very local NP distribution inside lysosomes. This valuable information would be then accessible by means of a simple macroscopic ZFC experiment.

The exposed model also suggests a new interpretation of the maximum of the ZFC curve not depending on the NP relaxation time as widely assumed but on the decrease of interaction effects with temperature.

Finally, the presented work only focuses on ZFC experiment and its interpretation. Nevertheless, the way the local field is analyzed is quite general and can presumably be used as a start to study how biomedical applications using magnetic NPs at room temperature are modified after the cellular internalization of NPs.

ACKNOWLEDGMENTS

We are grateful to F. Gendron for fruitful discussions and for his valuable assistance concerning the SQUID experiments. We acknowledge Guerbet and the laboratory PECSA (UMR7195, UPMC) (especially Christine Ménager and Sébastien Ballet) for providing us with the nanoparticles. We are indebted to Christine Pechoux and Sophie Chat for TEM observations and to Nathalie Luciani, Alain Luciani, and Vanessa Deveaux for animal experiments. This work has been supported by the Agence Nationale de la Recherche (ANR) TecSan "Inflam" and by the European project Magnifyco (Contract No. NMP4-SL-2009-228622).

*florence.gazeau@univ-paris-diderot.fr

[1] P. Gillis and S. H. Koenig, Magn. Reson. Med. **5**, 323 (1987).
[2] A. S. Arbab and J. A. Frank, Regen. Med. **3**, 199 (2008).
[3] M. Johannsen, U. Gneveckow, L. Eckelt, A. Feussner, N. Waldofner, R. Scholz, S. Deger, P. Wust, S. A. Loening, and A. Jordan, Int. J. Hyperther. **21**, 637 (2005).
[4] A. Jordan, R. Scholz, K. Maier-Hauff, M. Johannsen, P. Wust, J. Nadobny, H. Schirra, H. Schmidt, S. Deger, S. Loening, W. Lanksch, and R. Felix, J. Magn. Magn. Mater. **225**, 118 (2001).
[5] B. Thiesen and A. Jordan, Int. J. Hyperther. **24**, 467 (2008).
[6] C. Wilhelm and F. Gazeau, Biomaterials. **29**, 3161 (2008).
[7] M. Lévy, M. Devaud, N. Luciani, V. Deveaux, D. Elgrabli, F. Gendron, A. Luciani, C. Wilhelm, and F. Gazeau, ACS Nano. (submitted).
[8] J. M. Vargas, W. C. Nunes, L. M. Socolovsky, M. Knobel, and D. Zanchet, Phys. Rev. B **72**, 184428 (2005).
[9] S. Koutani, G. Gavoille, and R. Gérardin, J. Magn. Magn. Mater. **123**, 175 (1993).

[10]M. Knobel, W. C. Nunes, A. L. Brandl, J. M. Vargas, L. M. Socolovsky, and D. Zanchet, Physica B **354**, 80 (2004).
[11]J. L. Dormann, D. Fiorani, and E. Tronc, J. Magn. Magn. Mater. **202**, 251 (1999).
[12]S. Mørup and E. Tronc, Phys. Rev. Lett. **72**, 3278 (1994).
[13]M. F. Hansen and S. Mørup, J. Magn. Magn. Mater. **184**, 262 (1998).
[14]P. Allia, M. Coisson, P. Tiberto, F. Vinai, M. Knobel, M. A. Novak, and W. C. Nunes, Phys. Rev. B **64**, 144420 (2001).
[15]R. W. Chantrell, N. Walmsley, J. Gore, and M. Maylin, Phys. Rev. B **63**, 024410 (2000).
[16]M. Azeggagh and H. Kachkachi, Phys. Rev. B **75**, 174410 (2007).
[17]J. L. Dormann, R. Cherkaoui, L. Spinu, M. Nogues, F. Lucari, F. D'Orazio, D. Fiorani, A. Garcia, E. Tronc, and J. P. Jolivet, J. Magn. Magn. Mater. **187**, L139 (1998).
[18]M. F. Hansen, P. E. Jönsson, P. Norblad, and P. Svendinhl, J. Phys. Condens. Matter **14**, 4901 (2002).
[19]C. R. Vestal, Q. Song, and Z. J. Zhang, J. Phys. Chem. B **108**, 18222 (2004).
[20]M. Suzuki, S. I. Fullem, I. S. Suzuki, L. Wang, and C. J. Zhong, Phys. Rev. B **79**, 024418 (2009).
[21]N. Luciani, F. Gazeau, and C. Wilhelm, J. Mater. Chem. **19**, 6373 (2009).
[22]C. Wilhelm, F. Gazeau, and J. C. Bacri, Eur. Biophys. J. **31**, 118 (2002).
[23]C. Rivière, C. Wilhelm, F. Cousin, V. Dupuis, F. Gazeau, and R. Perzynski, Eur. Phys. J. E **22**, 1 (2007).
[24]A. Tanimoto and S. Kuribayashi, Eur. J. Radiol. **58**, 200 (2006).
[25]M. Lévy, N. Luciani, D. Alloyeau, D. Elgrabli, V. Deveaux, C. Pechoux, S. Chat, G. Wang, N. Vats, F. Gendron, C. Factor, S. Lotersztajn, A. Luciani, C. Wilhelm, and F. Gazeau, Biomaterials **32**, 3988 (2011).
[26]M. Lévy, F. Lagarde, V.-A. Maraloiu, M.-G. Blanchin, F. Gendron, C. Wilhelm, and F. Gazeau, Nanotechnology **21**, 395103 (2010).
[27]R. Sappey, E. Vincent, N. Hadacek, F. Chaput, J. P. Boilot, and D. Zins, Phys. Rev. B **56**, 14551 (1997).
[28]T. Bitoh, K. Ohba, M. Takamatsu, T. Shirane, and S. Chikazawa, J. Phys. Soc. Jpn. **64**, 1305 (1995).
[29]J. Dormann, Rev. Phys. Appl. **16**, 275 (1981).
[30]Y. Raikher and M. Shliomis, Adv. Chem. Phys. **87**, 595 (1994).
[31]W. F. Brown, Phys. Rev. **130**, 1677 (1963).
[32]C. Tannous and J. Gieraltowski, Eur. J. Phys. **29**, 475 (2008).
[33]W. T. Coffey, D. S. F. Crothers, J. L. Dormann, L. J. Geoghegan, Y. P. Kalmykov, J. T. Waldron, and A. W. Wickstead, Phys. Rev. B **52**, 15951 (1995).
[34]W. T. Coffey, D. S. F. Crothers, J. L. Dormann, Y. P. Kalmykov, E. C. Kennedy, and W. Wernsdorfer, Phys. Rev. Lett. **80**, 5655 (1998).
[35]S. A. Majetich and M. Sachan, J. Phys. D: Appl. Phys. **39**, R407 (2006).